European Journal of Nuclear Medicine and Molecular Imaging (2019) 46:1685–1694
https://doi.org/10.1007/s00259-019-04333-4

ORIGINAL ARTICLE

Advanced MR imaging and ^{18}F-DOPA PET characteristics of H3K27M-mutant and wild-type pediatric diffuse midline gliomas

Arnoldo Piccardo[1] · Domenico Tortora[2] · Samantha Mascelli[3] · Mariasavina Severino[2] · Gianluca Piatelli[4] · Alessandro Consales[4] · Marco Pescetto[5] · Veronica Biassoni[6] · Elisabetta Schiavello[6] · Michela Massollo[1] · Antonio Verrico[7] · Claudia Milanaccio[7] · Maria Luisa Garrè[7] · Andrea Rossi[2] · Giovanni Morana[2]

Received: 20 January 2019 / Accepted: 10 April 2019 / Published online: 27 April 2019

Abstract

Purpose The aim of this study was to investigate MRI-derived diffusion weighted imaging (DWI), ^{1}H-MR spectroscopy (^{1}H-MRS) and arterial spin labeling (ASL) perfusion imaging in comparison with ^{18}F-dihydroxyphenylalanine (DOPA) PET with respect to diagnostic evaluation of pediatric diffuse midline gliomas (DMG) H3K27M-mutant and wild-type.

Methods We retrospectively analyzed 22 pediatric patients with DMG histologically proved and molecularly classified as H3K27M-mutant (12 subjects) and wild-type (10 subjects) who underwent DWI, ^{1}H-MRS, and ASL performed within 2 weeks of ^{18}F-DOPA PET. DWI-derived relative minimum apparent diffusion coefficient (rADC min), ^{1}H-MRS data [choline/N-acetylaspartate (Cho/NAA), choline/creatine (Cho/Cr), and presence of lactate] and relative ASL-derived cerebral blood flow max (rCBF max) were compared with ^{18}F-DOPA uptake Tumor/Normal tissue (T/N) and Tumor/Striatum (T/S) ratios, and correlated with histological and molecular features of DMG. Statistics included Pearson's chi-square and Mann-Whitney U tests, Spearman's rank correlation and receiver operating characteristic (ROC) analysis.

Results The highest degrees of correlation among different techniques were found between T/S, rADC min and Cho/NAA ratio ($p < 0.01$), and between rCBF max and rADC min ($p < 0.01$). Significant differences between histologically classified low- and high-grade DMG, independently of H3K27M-mutation, were found among all imaging techniques ($p \leq 0.02$). Significant differences in terms of rCBF max, rADC min, Cho/NAA and ^{18}F-DOPA uptake were also found between molecularly classified mutant and wild-type DMG ($p \leq 0.02$), even though wild-type DMG included low-grade astrocytomas, not present among mutant DMG. When comparing only histologically defined high-grade mutant and wild-type DMG, only the ^{18}F-DOPA PET data T/S demonstrated statistically significant differences independently of histology ($p < 0.003$). ROC analysis demonstrated that T/S ratio was the best parameter for differentiating mutant from wild-type DMG (AUC 0.94, $p < 0.001$).

Conclusions Advanced MRI and ^{18}F-DOPA PET characteristics of DMG depend on histological features; however, ^{18}F-DOPA PET-T/S was the only parameter able to discriminate H3K27M-mutant from wild-type DMG independently of histology.

Andrea Rossi and Giovanni Morana are joint last authors.

Electronic supplementary material The online version of this article (https://doi.org/10.1007/s00259-019-04333-4) contains supplementary material, which is available to authorized users.

✉ Giovanni Morana
giovannimorana@gaslini.org

[1] Nuclear Medicine Unit, Ente Ospedaliero Ospedali Galliera, Genoa, Italy

[2] Neuroradiology Unit, IRCCS Istituto Giannina Gaslini, via G. Gaslini 5, 16147 Genoa, Italy

[3] Head-Neck and Neuroscience Department, IRCCS Istituto Giannina Gaslini, Genoa, Italy

[4] Neurosurgery Unit, IRCCS Istituto Giannina Gaslini, Genoa, Italy

[5] Anaesthesiology Department, Ente Ospedaliero Ospedali Galliera, Genoa, Italy

[6] Pediatric Unit, Fondazione IRCCS Istituto Nazionale dei Tumori, Milan, Italy

[7] Neuro-oncology Unit, IRCCS Istituto Giannina Gaslini, Genoa, Italy

Keywords DOPA PET · Magnetic resonance spectroscopy · Diffuse midline glioma · Arterial spin labeling · Diffusion weighted imaging

Introduction

In the revised 2016 World Health Organization (WHO) classification of tumors of the central nervous system, the diffuse midline glioma (DMG) H3K27M-mutant has been introduced as a completely new entity [1]. According to the rule "molecular pathology beats histopathology", the detection of H3K27M mutation, independently of the histological appearance (which could even be that of a low-grade diffusely infiltrating lesion), determines an assignment to WHO grade IV. Diffuse midline gliomas H3K27M-mutant predominate in children but can also be seen in adults, and grow in all midline central nervous system compartments with the most common locations being the brain stem, thalamus, and spinal cord. For DMG in general, the finding of an H3K27M mutation confers a worse prognosis than that of wild-type cases [1].

Over the past few years, a number of tumors that are not DMG (including ependymomas, pilocytic astrocytomas and gangliogliomas) have been reported to harbor the same H3K27M mutation, although the prognostic significance remains unelucidated [2]. For these reasons, cIMPACT-NOW (the Consortium to Inform Molecular and Practical Approaches to CNS Tumor Taxonomy) Working Committee 3 recently provided updated recommendations in order to clarify diagnostic criteria of DMG, which should only include infiltrating midline gliomas [2].

A recent study evaluated the structural MRI characteristics of pediatric DMG without evidence of distinguishing features among H3K27M-mutant and wild-type lesions [3]. No prior studies have so far evaluated or compared advanced MRI features and metabolic information obtained by ^{18}F-dihydroxyphenylalanine (DOPA) PET focusing on this new entity. Prior studies in diffuse astrocytic tumors have demonstrated that these techniques significantly improve the understanding of the physiopathology of pediatric gliomas and provide significant information for tumor characterization, treatment monitoring and outcome prediction [4–7].

On the basis of these considerations, the aim of this retrospective study was to analyze the advanced MR imaging features obtained by diffusion weighted imaging (DWI), ^{1}H-MR spectroscopy (^{1}H-MRS) and arterial spin labeling (ASL) perfusion imaging in comparison with ^{18}F-DOPA PET in a group of children with H3K27M-mutant and wild-type DMG. Specifically, we aimed to evaluate the degree of correlation between these methods and test their ability in discriminating H3K27M-mutant from wild-type DMG.

Materials and methods

Patient population

We retrospectively evaluated all consecutive pediatric patients (aged less than 18 years at diagnosis) referred to our Institution between 2010 and 2018 for newly diagnosed treatment naïve (except biopsy) DMG who underwent MRI (including DWI, ^{1}H-MRS and ASL) and ^{18}F-DOPA PET within 2 weeks of each other. Twenty-two (12 males and 10 females) subjects were identified. Patient age ranged from 4 to 17 years (median, 9 years). Six of these patients had been previously included in retrospective studies aimed at comparing metabolic information obtained by ^{18}F-DOPA PET and ^{1}H-MRS in pediatric supratentorial infiltrative gliomas or to analyze diagnostic information obtained by MRI DWI and ASL perfusion imaging in comparison with ^{18}F-DOPA PET in supratentorial and infratentorial pediatric astrocytic tumors [7, 8].

The main characteristics of patients and their brain lesions are summarized in Table 1. Information reviewed for each subject included histology and molecular features. In particular, molecular analyses were performed to test the presence of mutations in the histone variants H3.3 (H3F3A) and H3.1 (HIST1H3B). Tumor grading was determined according to the revised 2016 WHO criteria [1].

Overall there were 12 subjects with WHO grade IV DMG H3K27M-mutant (5 patients with glioblastomas and 7 with anaplastic astrocytomas) and ten subjects with H3K27M wild-type DMG (3 glioblastomas WHO grade IV, 3 anaplastic astrocytomas WHO grade III, and 4 diffuse astrocytomas WHO grade II). All subjects with DMG H3K27M-mutant presented mutations in the histone variant H3.3 (H3F3A). The Regional Ethics committee of Liguria, Genoa, Italy, approved the retrospective data evaluation.

Image protocol and analysis

PET data acquisition was carried out with a PET/CT Discovery ST system (GE Healthcare, Milwaukee, WI, USA). Data were acquired as previously reported [7, 8] in 3-dimensional mode with a scanning time of 30 min. The participants fasted for at least 4 h before ^{18}F-DOPA administration (IASOdopa®, IASON Labormedizine Ges. Mbh & Co. KG, Graz-Seiersberg, Austria). The median injected activity was 100 MBq (range 74–185 MBq according to body weight). Images were acquired 20 min after ^{18}F-DOPA administration.

Table 1 Patient characteristics and imaging findings

Case	Age at diagnosis (year)	Sex	Diagnosis	Location	WHO Grade	CE (Y/N)	NA (Y/N)	rCBF max	rADC min	Cho / NAA	Cho / Cr	Lac (±)	T/N	T/S
1	12	M	DMG, H3K27M-m (GB)	L-DMJ	IV	N	N	1.41	0.90	3.54	3.52	+	2.50	1.50
2	4	M	DMG, H3K27M-m (GB)	R-Th / L-Th	IV	Y	Y	2.34	0.76	4.47	2.20	–	2.60	1.60
3	10	M	DMG, H3K27M-m (GB)	Pons	IV	Y	Y	1.15	0.87	15.25	2.86	–	3.20	2.00
4	12	F	DMG, H3K27M-m (GB)	Medulla	IV	N	N	1.90	0.95	7.15	1.39	–	2.80	1.80
5	7	F	DMG, H3K27M-m (GB)	R-DMJ	IV	Y	Y	1.80	0.86	3.80	9.70	–	2.30	1.60
6	7	M	DMG, H3K27M-m (AA)	Pons	IV	N	N	2.80	0.76	4.50	2.40	–	2.20	1.34
7	9	F	DMG, H3K27M-m (AA)	Pons	IV	N	N	2.00	1.12	1.97	3.12	–	2.61	1.33
8	17	F	DMG, H3K27M-m (AA)	R-DMJ/Pons	IV	Y	N	2.00	0.80	2.64	3.35	–	2.70	1.40
9	11	F	DMG, H3K27M-m (AA)	Pons	IV	Y	N	2.25	0.78	12.40	4.23	–	2.90	1.65
10	12	F	DMG, H3K27M-m (AA)	R-Th	IV	Y	Y	2.07	0.79	2.22	1.91	–	2.32	1.21
11	4	F	DMG, H3K27M-m (AA)	R-Th	IV	N	N	1.39	0.76	11.52	2.40	–	4.50	2.10
12	14	F	DMG, H3K27M-m (AA)	R-Th	IV	Y	N	1.62	0.88	8.25	3.19	–	3.18	1.48
13	9	M	GB, H3K27M-wt	R-Th	IV	Y	Y	1.37	0.78	5.00	4.24	–	2.00	1.20
14	6	M	GB, H3K27M-wt	L-Th	IV	Y	Y	1.50	0.91	5.42	9.45	+	2.22	1.11
15	9	M	GB, H3K27M-wt	L-Th	IV	Y	Y	2.20	0.86	2.36	2.69	+	3.00	1.35
16	17	F	AA, H3K27M-wt	R-Th / L-Th	III	N	N	1.60	1.06	4.24	1.66	–	3.30	1.40
17	8	M	AA, H3K27M-wt	Pons	III	N	N	0.80	1.42	0.80	1.54	–	1.00	0.60
18	10	M	AA, H3K27M-wt	R-Th / L-Th	III	N	N	1.40	0.82	1.40	1.10	+	1.90	1.11
19	5	M	DA, H3K27M-wt	R-Th / L-Th	II	N	N	0.90	1.18	3.80	1.97	+	1.00	0.60
20	14	M	DA, H3K27M-wt	R-Th	II	N	N	0.73	1.55	1.34	1.13	–	0.90	0.50
21	6	M	DA, H3K27M-wt	Pons	II	N	N	0.78	1.26	0.93	1.08	–	0.95	0.45
22	9	F	DA, H3K27M-wt	Medulla-CSC	II	N	N	0.73	1.23	1.05	1.86	–	1.00	0.60

CE contrast enhancement, *NA* necrotic areas, *Lac* lactate, *Y* yes, *N* no, *M* male, *F* female, *DMG* diffuse midline glioma, *GB* glioblastoma, *AA* anaplastic astrocytoma, *DA* diffuse astrocytoma, *DMJ* diencephalic-mesencephalic junction, *wt* wildtype, *m* mutant, *R* right, *L* left, *Th* thalamus, *CSC* cervical spinal cord

Carbidopa premedication was not utilized. A non-diagnostic low dose CT scan was used for attenuation correction.

MRI studies were performed on a 1.5 Tesla magnet (Intera Achieva; Philips, Best, the Netherlands) using an 8-channel head array receiving coil for sensitivity encoding (SENSE) parallel imaging. Each patient received routine clinical MRI scans including pre-contrast axial Spin Echo (SE) T1-weighted images, Fluid Attenuation Inversion Recovery (FLAIR) and axial and coronal Turbo Spin Echo (TSE) T2-weighted images. Following gadolinium compound bolus administration (0.1 mmol/kg, macrocyclic ionic agent) axial, coronal, and sagittal SE T1-weighted images along with an

axial 3D T1-weighted sequence for neuronavigation purposes were acquired.

DWI was performed using a single-shot spin-echo (SE) echo-planar sequence (TR/TE = 5.050/63 ms; 90° flip angle; NEX = 1, 30 transverse sections; SENSE factor = 2.5; slice thickness/gap = 4 mm/1 mm; FOV = 160 mm; 100 × 160 matrix; acquisition time of 1 min 9 s). ADC maps were automatically calculated from the b = 0 and b = 1.000 s/mm^2 DWI series by the MRI scanner software.

ASL was implemented using signal targeting and alternating radiofrequency (EPISTAR) with pulsed arterial spin labeling and a multi-slice single-shot echo planar imaging (EPI) readout with parallel imaging (SENSE factor = 2.3; TR/TE, 4000/25 ms; flip angle, 40°; matrix size, 80 × 77; FOV, 240 × 240 mm; slice thickness/gap = 5 mm/0; 22 axial sections; 30 label/control pairs; 100 mm labeling slab thickness with a gap of 20 mm; label delay ranging between 1500 and 1800 ms according to patient age; scan time of 4 min 8 s). ASL imaging was done without using crusher gradients.

^{1}H-MRS was performed using a single-voxel point resolved spectroscopy (PRESS) technique with an intermediate echo time of 144 milliseconds, repetition time of 2000 milliseconds, and 128 signal averages. With these parameters, the total acquisition time, including scanner adjustments, was less than 5 min. A cubic voxel of 1.8 cm side length was manually placed on the bulk of the lesion, according to standard diagnostic criteria, to enclose only tumor tissue and avoid or limit the inclusion of necrotic areas as much as possible.

Images were analyzed on a dedicated workstation (OsiriX, Pixmeo SARL, Bernex, Switzerland) which also allowed co-registration of ^{18}F-DOPA PET and MRI images as previously described [7]. In detail, for each case, PET images were first visually inspected and the axial image slice displaying the maximum tumor uptake was selected avoiding, whenever present, developmental venous anomalies [9]; a circular ROI of 8 mm diameter was manually drawn over the tumor (T) area with the peak activity. In case of negligible ^{18}F-DOPA uptake, the ROI was placed in the center of the lesion [7, 10]. The radiotracer concentration in the ROI was normalized to the injected dose per patient body weight, and the maximum standardized uptake value (SUVmax) was obtained for each lesion [maximum pixel value (kBq/mL) within the ROI / injected dose (kBq) / patient weight (g)]. For the normal background (N) reference tissue, a large circular ROI (diameter 50 mm) was drawn in the normal cerebral hemisphere at the level of the centrum semiovale, including cortical and white matter. In subjects with midline gliomas involving the right or left thalamus the contralateral normal cerebral hemisphere was selected whereas in all patients with bi-thalamic lesions or brainstem lesions the normal left cerebral hemisphere was selected. An additional ROI (diameter, 8 mm) was drawn over the normal striatum (S). Ratios of tumor to normal tissue uptake were generated by dividing the tumor SUVmax by the SUVmax of the normal brain region (T/N) and of the normal striatum (T/S). Then, diffusion and perfusion measurements were obtained from co-registered MRI/PET scans as previously described [7, 11]. In detail, the maximum tumoral cerebral blood flow (CBF max) and minimum apparent diffusion coefficient (ADC min) were measured by placing an 8-mm diameter circular region of interest (ROI) on the CBF and ADC maps in the region corresponding to the PET hotspot area; we then evaluated whether that ROI corresponded to the maximum CBF and minimum ADC. To do so, the ROI was systematically moved outside the PET hotspot region in all tumor slices in order to measure regions with higher perfusion and lower diffusion, respectively, and to obtain CBF max and ADC min for each case. Careful attention was paid to avoid blood vessels, necrosis, and hemorrhage. Finally, the relative tumoral maximum cerebral blood flow (rCBF max) was obtained by normalizing the CBF max by a blood flow measurement from a reference region in the same area used for determining T/N. The same procedure was used to obtain relative minimum ADC values (rADC min). In case of negative ^{18}F-DOPA PET, the ROI was first placed in the center of the lesion and then systematically moved within the tumoral area as depicted by FLAIR imaging in order to measure regions with the highest perfusion and lowest diffusion.

^{1}H-MRS data were generated by the internal scanner software, providing automatic peak assignation and ratio calculation. Choline-to-creatine (Cho/Cr) and choline-to-N-acetylaspartate (Cho/NAA) peak area ratios were recorded. For each ^{1}H-MRS study, presence of lactate, defined by prominent peak (signal: noise >3:1) between 1.3 and 1.4 ppm, was also assessed. Metabolic data obtained by the ^{1}H-MRS volume of interest (VOI) in the bulk of the lesion were compared with rADC min, rCBF max, T/S and T/N.

The MRI contrast enhancement pattern of the lesions was also reviewed (presence or absence of contrast enhancement and necrotic areas).

Statistical analysis

Descriptive statistics included mean, standard deviation, minimum, and maximum of continuous factors and scores; in the case of categorical factors, number and percentage distribution were used. Pearson's chi-square and Mann-Whitney U tests were used to compare categorical and continuous factors, respectively. In the first level of the analysis the Spearman's rank coefficient was used to test the correlations between rCBF max, rADC min, Cho/Cr, Cho/NAA, T/S and T/N. To test the performance of these parameters in their ability to differentiate between mutant and wild-type DMG a receiver operating characteristic (ROC) curve analysis was applied. A cutoff value for each parameter was determined by maximizing the sum of sensitivity and specificity.

ROC curve analysis was performed with MedCalc software, version 12.5 (MedCalc Software, Ostend, Belgium). All other statistical analyses were conducted by using SPSS Statistic software, version 21 (IBM, Armonk, NY) and STATA software, version 14 (StataCorp, College Station, TX). Two-tailed probabilities are reported and a p value of 0.05 was used to define nominal statistical significance.

Results

A significant positive correlation was demonstrated between perfusion imaging (rCBF max) and the T/S and T/N ^{18}F-DOPA PET parameters. There was no significant correlation between rCBF max and ^{1}H-MRS data. A significant negative correlation was found between diffusion weighted imaging (rADC min) and rCBF max, the T/S ^{18}F-DOPA PET data, and ^{1}H-MRS data Cho/Cr and Cho/NAA. In addition to rCBF max, T/S and T/N ^{18}F-DOPA PET data demonstrated a significant positive correlation with ^{1}H-MRS data, with the exception between T/N and Cho/Cr. The highest degrees of positive correlation among different techniques were found between Cho/NAA ratio and ^{18}F-DOPA PET data, whereas the highest degrees of negative correlation were between rADC min and rCBF max and between rADC min and T/S ($p < 0.01$). The strongest linear correlation among different techniques (Spearman's rho: 0.75) was demonstrated between T/S and Cho/NAA ratio (Online Resource, Supplementary Table 1).

MRI derived contrast enhancement pattern, rCBF max, rADC min, Cho/Cr and Cho/NAA ratios, and ^{18}F-DOPA PET uptake (T/S and T/N) data of all lesions are reported in Table 1.

Significant differences between histologically classified low- and high-grade DMG, independently of H3K27M mutation, were found among all imaging techniques ($p \leq 0.02$). When comparing molecularly classified H3K27M-mutant and wild-type DMG, significant differences in terms of rCBF max, rADC min, Cho/NAA, and ^{18}F-DOPA uptake were found. No significant differences, but a suggestive trend, emerged for Cho/Cr ($p = 0.06$). In detail, H3K27M-mutant DMG demonstrated significantly lower rADC min values on DWI ($p = 0.01$), higher rCBF max on ASL PWI ($p = 0.004$), higher Cho/NAA ratios on ^{1}H-MRS ($p = 0.02$) and higher T/S ($p < 0.001$) and T/N ratios ($p = 0.009$) on ^{18}F-DOPA PET (Table 2).

ROC analysis indicated that the T/S ratio showed the highest area under the curve (AUC) value (AUC 0.94, sensitivity 83%, specificity 60%, $p < 0.001$), and the Cho/NAA ratio the lowest AUC value (AUC 0.78, sensitivity 100%, specificity 80%, $p = 0.004$). However, there was no significant difference in the diagnostic performances of these continuous variables for differentiating H3K27M-mutant and wild-type DMG according to pairwise comparison of ROC curves. Threshold analysis of the ROC data are reported in Table 2. ROC curves are reported in Online Resource, Supplementary Fig. 1.

A lactate peak on ^{1}H-MRS was found in 4/10 H3K27M wild-type DMG (one diffuse astrocytoma, one anaplastic astrocytoma, and two glioblastomas) and in only 1 out of 12 H3K27M-mutant DMG (one glioblastoma), approaching, although not reaching, statistical significance ($p = 0.08$).

Regarding the contrast enhancement pattern, no significant differences in terms of presence of contrast enhancement ($p = 0.18$) and necrotic areas ($p = 0.61$) were found between H3K27M-mutant and wild-type DMG.

Nevertheless, since wild-type DMG included low-grade diffuse astrocytomas, not present among H3K27M-mutant DMG, we performed an additional analysis to compare only histologically defined high-grade mutant and wild-type DMG. On this analysis, only the ^{18}F-DOPA PET data T/S demonstrated statistically significant differences independently of histology ($p = 0.003$) between mutant and wild-type DMG. ROC analysis indicated that the T/S ratio showed an AUC value of 0.91, sensitivity 75%, specificity 83%, $p < 0.001$ (Table 3).

Representative images of H3K27M-mutant and wild-type DMG are shown in Fig. 1.

Discussion

No prior studies focusing on pediatric patients with H3K27M-mutant and wild-type DMG have so far evaluated diagnostic information gathered by advanced MRI techniques including DWI, ^{1}H-MRS and ASL. In addition, no prior studies have compared information provided by advanced MRI techniques with ^{18}F-DOPA PET.

H3K27M mutation is caused by the conversion of a lysine to methionine at residue 27, inducing unique gain-of-function mechanisms that lead to lower overall amounts of H3 with trimethylated lysine 27 (H3K27me3). Functional analysis has highlighted the role of H3K27M as contributing to abnormal cell-cycle control, inhibition of autophagy, and potentially augmenting tumor resistance to radiotherapy [12, 13]. However, the precise role of H3K27M in tumor initiation remains undefined as it is not sufficient on its own for tumorigenesis in vivo [12, 14].

In our series, all H3K27M-mutant DMG presented mutations of the histone H3.3 gene (H3F3A). Castel et al. have proposed that within the H3K27M-mutant DMG, differences in tumorigenic pathway and biology exist between H3.1 and H3.3 mutations, with H3.3 mutations portending a worse prognosis [15]. Given the known correlation between histone mutations and outcome, in DMG there is an increased tendency to search for non-invasive biomarkers that might correlate with molecular data (i.e. liquid biopsy) [16]. Imaging biomarkers provide the advantage of evaluating the entire lesion over the typically limited extent of surgical biopsies. The potential

Table 2 Statistical results of ^{18}F-DOPA PET data (T/S and T/N) and MRI derived DWI (rADC min), ASL (rCBF max) and ^{1}H-MRS (Cho/NAA and Cho/Cr) for a two-tiered classification for H3K27M-mutant and wild-type DMG

Variable	H3K27M-m [a] ($n = 12$)	H3K27M-wt [a] ($n = 10$)	P value[b]	AUC	IC_AUC	Cut-off	Sensitivity (%)	Specificity (%)	P value[c]
T/S	1.58 ± 0.27	0.89 ± 0.37	<0.001	0.94	0.75-0.99	>1.20	83	60	<0.001
T/N	2.80 ± 0.61	1.72 ± 0.90	0.009	0.82	0.60-0.95	>2.20	91	80	0.004
rADC min	0.85 ± 0.10	1.10 ± 0.26	0.011	0.81	0.59-0.94	<0.88	83	70	0.001
rCBF max	1.89 ± 0.45	1.20 ± 0.49	0.004	0.85	0.63-0.96	>1.40	83	72	<0.001
Cho/NAA	6.47 ± 4.45	2.63 ± 1.80	0.02	0.78	0.56-0.93	>2.36	100	80	0.004
Cho/Cr	3.35 ± 2.14	2.67 ± 2.56	0.06	*	*	*	*	*	*

[*] ROC analysis not performed because of lack of statistically significant differences on Mann-Whitney U Test

[a] Data are reported as the mean ± standard deviation

[b] Value for the difference between H3K27M-mutant and wild-type DMG according to two-tiered classification

[c] Value for ROC analysis

benefit to non-invasively discriminate H3K27M-mutant from wild-type DMG would be especially important in diffuse intrinsic pontine gliomas where biopsy is not yet routinely performed; at the same time, since in DMG complete surgical removal is impossible and given the possibility of inaccurate results when biopsy samples are not taken from the most malignant region, non-invasive evaluation of the microstructural, microvascular and metabolic heterogeneity of the entire lesion

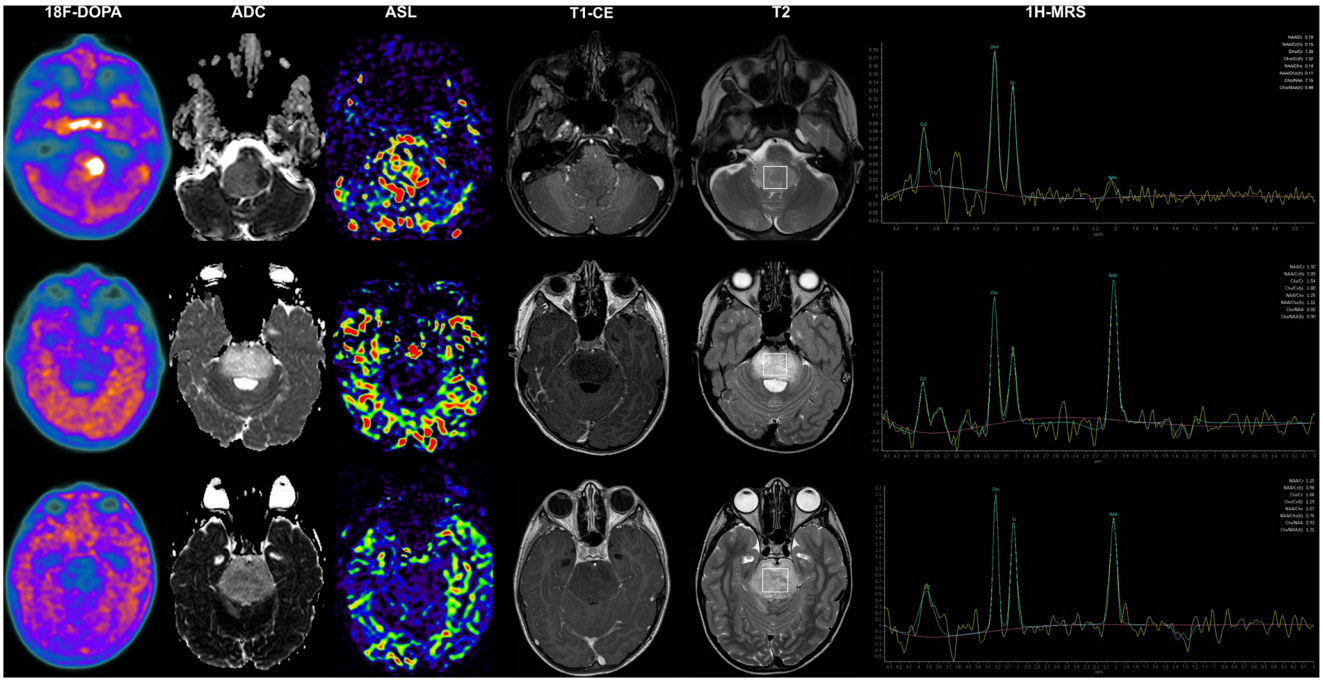

Fig. 1 ^{18}F-DOPA PET and MRI images of H3K27M-mutant and wild-type DMG. Upper row: DMG, H3K27M-m (GB), WHO grade IV (case 4) ^{18}F-DOPA PET shows an area of markedly increased uptake within the lesion (T/N: 2.80; T/S: 1.80). ADC demonstrates a focal area with mildly reduced diffusivity (rADC min: 0.95) on the left side of the lesion corresponding to the ^{18}F-DOPA PET hot spot region. ASL shows increased perfusion (rCBF max: 1.90). Contrast-enhanced (CE) T1-weighted image does not show contrast enhancement. ^{1}H-MRS demonstrates marked increase of Cho/NAA (7.15) and mild increase of Cho/Cr (1.39) ratios. Middle row: Diffuse intrinsic pontine glioma (AA), H3K27M-wt, WHO grade III (case 17) ^{18}F-DOPA PET shows absence of tracer uptake in the lesion (T/N: 1.00; T/S: 0.60). ADC demonstrates increased diffusion (rADC min: 1.42). ASL shows low perfusion (rCBF max: 0.80). CE T1-weighted image does not show contrast enhancement. ^{1}H-MRS demonstrates normal Cho/NAA (0.80) and mild increase of Cho/Cr (1.54) ratios. Of note, this was the only histologically defined high grade glioma which demonstrated lack of increased ^{18}F-DOPA uptake. Lower row: Diffuse intrinsic pontine glioma (DA), H3K27M-wt, WHO grade II (case 21) ^{18}F-DOPA PET shows absence of tracer uptake in the lesion (T/N: 0.95; T/S: 0.45). ADC and ASL images demonstrate increased diffusion (rADC min: 1.26) and low perfusion (rCBF max: 0.78). CE T1-weighted image does not show contrast enhancement. ^{1}H-MRS demonstrates normal Cho/NAA (0.93) and Cho/Cr (1.08) peak area ratios. Note: the box on T2-weighted images indicates the region of interest from which the spectra were acquired

Table 3 Statistical results of ^{18}F-DOPA PET data (T/S and T/N) and MRI derived DWI (rADC min), ASL (rCBF max) and ^{1}H-MRS (Cho/NAA and Cho/Cr) for a two-tiered classification for histologically defined high-grade H3K27M-mutant and wild-type DMG

Variable	H3K27M-m[a] ($n = 12$)	H3K27M-wt[a] ($n = 6$)	P value[b]	AUC	IC_AUC	Cut-off	Sensitivity (%)	Specificity (%)	P value[c]
T/S	1.58 ± 0.27	1.12 ± 0.28	0.003	0.91	0.68-0.99	>1.35	75	83	<0.001
T/N	2.80 ± 0.61	2.23 ± 0.82	0.18	*	*	*	*	*	*
rADC min	0.85 ± 0.10	0.97 ± 0.23	0.21	*	*	*	*	*	*
rCBF max	1.89 ± 0.45	1.47 ± 0.45	0.10	*	*	*	*	*	*
Cho/NAA	6.47 ± 4.45	3.20 ± 1.94	0.18	*	*	*	*	*	*
Cho/Cr	3.35 ± 2.14	3.44 ± 3.14	0.55	*	*	*	*	*	*

[a] Data are reported as the mean ± standard deviation

[b] Value for the difference between histologically defined high-grade H3K27M-mutant and wild-type DMG according to two-tiered classification

[c] Value for ROC analysis

[*] ROC analysis not performed because of lack of statistically significant differences on Mann-Whitney U Test

could be extremely helpful to suggest the biopsy site, so as to sample the most representative component of the tumor. Furthermore, due to risks, costs, and clinical regulations associated with the procedure, re-biopsy is rarely performed at disease progression. A recent study demonstrated that liquid biopsy approach provides a molecularly based tool for tumor characterization, indicating also clinical utility for longitudinal surveillance of DMG [17]. Since imaging is necessary for longitudinal surveillance, the identification of imaging biomarkers that may correlate with molecular data might also be useful for treatment monitoring.

A recent study evaluated the conventional MRI characteristics of pediatric DMG based on histone H3K27M mutational status, but differentiating features based on conventional MRI that would help distinguish histone H3K27M-mutant from wild-type tumors were not identified [3]. However, in this study histological data were not provided. In our study we included and analyzed both histological and molecular characteristics of DMG to evaluate the potential role of microstructural, microvascular and metabolic information gathered by ADC derived from DWI, CBF derived from ASL, Cho/Cr, Cho/NAA and presence of lactate derived from ^{1}H-MRS in comparison with metabolic information offered by ^{18}F-DOPA PET in predicting molecular features of DMG, independently of histology.

Our analysis confirmed the results of prior researches performed with these techniques in discriminating pediatric low-grade from high-grade diffusely infiltrating gliomas on the basis of histological features [7, 8, 10, 18–21]. All low-grade midline diffuse astrocytomas in this series, including one diffuse intrinsic pontine glioma, one diffusely infiltrating astrocytoma involving the junction between the medulla and the cervical spinal cord and two thalamic diffuse astrocytomas, demonstrated increased diffusivity, hypoperfusion, lack of increased ^{18}F-DOPA PET uptake, and a predominant pattern of mild increase of Cho/Cr and Cho/NAA ratios; on the other hand, all but one histologically defined high-grade DMG, independently of the presence or absence of H3K27M-mutation, demonstrated statistically different results in all imaging techniques. These data indicate that advanced MRI and ^{18}F-DOPA PET characteristics of pediatric DMG are strongly dependent on the histological features of the lesion, as previously demonstrated also in off-midline diffusely infiltrating astrocytomas [7, 8, 10, 22].

DWI provides information regarding diffusion of water molecules in the section studied, from which quantitative values, the so-called apparent diffusion coefficient (ADC), can be calculated providing non-invasive estimation of differences in cell density and tissue structure. ADC values derived from DWI have been shown to be decreased in highly cellular tumors, such as pediatric high-grade gliomas [23].

ASL is a perfusion method providing quantitative measurements of hemodynamic properties of the brain at the microcirculation level, exploiting arterial water as a freely diffusible tracer [24]. This technique provides quantification of cerebral blood flow and displays a high potential in evaluating pediatric brain gliomas, as demonstrated in prior studies in which increased perfusion of high-grade diffusely infiltrating astrocytomas correlated with enhanced microvascular density [18, 19, 23].

When compared to Dynamic Susceptibility Contrast (DSC) perfusion weighted imaging (PWI), currently the most commonly used method for evaluating brain tumor perfusion especially in adults, a recent study demonstrated a significant correlation between ASL and DSC PWI with respect to diagnostic performance in tumor grading in pediatric patients with low- and high-grade astrocytic tumors [25]. Similar results were demonstrated in another more recent study, in which a significant correlation between MRI perfusion metrics measured by DSC and ASL in pediatric brain tumors was found [26]. ASL-based CBF may therefore represent a viable biomarker for analysis of blood perfusion in pediatric astrocytic tumors and may be considered

an alternative to DSC PWI. Furthermore, ASL is also easy to implement on follow-up studies in children under chemotherapy treatment with difficult vascular access.

^{1}H-MRS allows non-invasive detection and estimation of normal and abnormal metabolites within brain tissue. Different patterns of metabolite concentrations are associated with loss of neuroaxonal integrity, increased myelin turnover, necrosis, or normal tissue [4]. ^{1}H-MRS is presently largely available on clinical MRI scanners and can be performed automatically in most situations. Prior studies involving pediatric diffuse astrocytic tumors demonstrated significant differences on ^{1}H-MRS ratios between high-grade and low-grade gliomas, with higher Cho/NAA and Cho/Cr ratios in high-grade lesions [27, 28].

Among amino-acid PET tracers, ^{18}F-DOPA has demonstrated high potential in defining tumor grade in pediatric infiltrative astrocytomas [7, 8, 10]. Increased ^{18}F-DOPA uptake has been shown to correlate with an overexpression of amino-acid transporters within regions of high proliferation with increased use of amino-acids for energy, protein synthesis, and cell division. Of note, concerning ^{18}F-DOPA PET imaging in differentiating low- from high-grade diffusely infiltrating pediatric gliomas, all low-grade DMG demonstrated a T/S ratio < 1 and all but one high-grade a T/S ratio > 1.

When comparing all lesions on the basis of the molecular classification, significant differences also emerged between all techniques. ROC analysis demonstrated a higher diagnostic performance for the ^{18}F-DOPA PET parameter T/S (higher AUC) when compared to DWI, ^{1}H-MRS and ASL; the Cho/NAA ratio showed the lowest AUC value even though statistical significance was not reached. These data are in line with prior investigations in children with supratentorial infiltrative gliomas, in which ^{1}H-MRS data, albeit reaching a statistical significance, demonstrated a greater degree of overlap among different glioma grades when compared to ^{18}F-DOPA uptake ratios [8]. Furthermore, Cho/Cr ratio did not show statistically significant differences between wild-type and mutant DMG.

Nevertheless, considering the significant differences between histologically defined low- and high-grade lesions among all techniques, the above reported results might have been influenced by the presence of low-grade diffuse astrocytomas in the group of wild-type DMG. When we compared only histologically defined high-grade gliomas with or without H3K27M mutation, ^{18}F-DOPA PET was the only technique which demonstrated statistically significant differences between mutant and wild-type DMG independently of histology. H3K27M-mutant anaplastic astrocytomas and glioblastomas demonstrated significantly higher T/S ratios when compared to wild-type high grade DMG. Since the finding of an H3K27M mutation confers a worse prognosis, the promising role of this imaging biomarker merits further investigation given the possibility to provide non-invasive information for tumor characterization, potentially even during treatment monitoring.

In our experience, the T/S ratio is extremely helpful in a clinical diagnostic setting to estimate pediatric diffuse astrocytic tumor aggressiveness and, unlike other amino-acid PET tracers, it allows to further stratify tumor uptake. Furthermore, according to the recently published guidelines in interpreting and quantifying results of brain ^{18}F-DOPA PET imaging in patients with gliomas, the striatum is the only recommended reference region for semiquantitative measures of ^{18}F-DOPA PET activity [29].

Interestingly, the presence of lactate, independently of the histological features of the tumor, was more frequent in wild-type DMG, demonstrating a trend toward significance; even though prior results have demonstrated lack of correlation between the presence of lactate and pediatric glioma grade [8], this element has never been explored or evaluated in prior studies involving DMG and deserves larger cohorts in order to establish its potential diagnostic role, supporting the known added value and synergistic role of multimodal multiparametric PET/MR imaging for pediatric diffuse astrocytic tumor characterization [7].

The strongest linear correlation among different techniques was demonstrated between T/S and Cho/NAA ratio. This ratio has been considered the most sensitive index for tumor cell density and proliferation in prior ^{1}H-MRS studies [30]. However, Cho/NAA did not show statistically significant differences between high grade wild-type and mutant DMG.

Among the limitations of our study, we are aware of its retrospective nature and of the relatively small sample of patients; however, we included only pediatric patients with midline diffuse astrocytic tumors, histologically and molecularly classified, studied with ASL, ^{1}H-MRS and ^{18}F-DOPA PET (other than DWI), which do not represent widespread diagnostic techniques in children, particularly for a single center. Of note, our cohort constitutes the first and largest series of pediatric DMG so far studied with these techniques. We acknowledge that ASL studies were performed on a 1.5-T MRI scanner; despite current recommendations for ASL [31] which advise the use of 3.0-T MRI, a recent study demonstrated that normalized pulsed ASL performed with a 1.5 T scanner provides comparable results to DSC MRI perfusion in pediatric astrocytic tumors, and may allow distinction between high- and low-grade lesions [25]. In addition, our data were acquired with an identical magnetic field strength recently adopted in the largest ASL study so far published in children with brain tumors, which demonstrated the reproducibility of CBF values between 1.5- and 3.0-T MRI [19]. We also recognize that single-voxel ^{1}H-MRS is unable to define the extent of the metabolic abnormalities in large tumors or demonstrate tissue heterogeneity. However, this technique provides robust and good-quality spectra in a relatively short period of time, compatible with standard clinical settings and patient compliance.

Conclusion

DWI, ASL, ^{1}H-MRS and ^{18}F-DOPA PET demonstrated significant differences between wild-type and mutant DMG prevailingly depending on the histological features of the lesions, since the results were probably influenced by the fact that low-grade diffuse astrocytomas were present only among wild-type lesions. However, a comparison including only histologically defined high-grade DMG showed significant differences in the ^{18}F-DOPA PET T/S ratio between H3K27M-mutant and wild-type lesions, highlighting the potential role of this parameter to non-invasively determine the H3K27M mutation status independently of histology. Larger studies are warranted to investigate this further and the role of amino-acid metabolism in H3K27M-mutant DMG. Further investigations on larger series are also awaited to elucidate the significance of lactate on ^{1}H-MRS in discriminating wild-type from mutant DMG.

Compliance with ethical standards

Conflict of interest The authors declare that they have no conflict of interest.

This article does not contain any studies with animals performed by any of the authors.

All procedures performed in studies involving human participants were in accordance with the ethical standards of the institutional and/or national research committee and with the 1964 Helsinki declaration and its later amendments or comparable ethical standards.

Informed consent was obtained from all individual participants or their legal guardians included in the study, and patient assent was obtained whenever appropriate.

References

1. Louis DN, Perry A, Reifenberger G, von Deimling A, Figarella-Branger D, Cavenee WK, et al. The 2016 World Health Organization classification of tumors of the central nervous system: a summary. Acta Neuropathol. 2016;131:803–20.
2. Louis DN, Giannini C, Capper D, Paulus W, Figarella-Branger D, Lopes MB, et al. cIMPACT-NOW update 2: diagnostic clarifications for diffuse midline glioma, H3 K27M-mutant and diffuse astrocytoma/anaplastic astrocytoma, IDH-mutant. Acta Neuropathol. 2018;135:639–42.
3. Aboian MS, Solomon DA, Felton E, Mabray MC, Villanueva-Meyer JE, Mueller S, et al. Imaging characteristics of pediatric diffuse midline gliomas with histone H3 K27M mutation. AJNR Am J Neuroradiol. 2017;38:795–800.
4. Mabray MC, Barajas RF Jr, Cha S. Modern brain tumor imaging. Brain Tumor Res Treat. 2015;3:8–23.
5. Rossi A, Gandolfo C, Morana G, Severino M, Garrè ML, Cama A. New MR sequences (diffusion, perfusion, spectroscopy) in brain tumours. Pediatr Radiol. 2010;40:999–1009.
6. Morana G, Piccardo A, Garrè ML, Nozza P, Consales A, Rossi A. Multimodal magnetic resonance imaging and 18F-L-dihydroxyphenylalanine positron emission tomography in early characterization of pseudoresponse and nonenhancing tumor progression in a pediatric patient with malignant transformation of ganglioglioma treated with bevacizumab. J Clin Oncol. 2013;31:e1–5.
7. Morana G, Piccardo A, Tortora D, Puntoni M, Severino M, Nozza P, et al. Grading and outcome prediction of pediatric diffuse astrocytic tumors with diffusion and arterial spin labeling perfusion MRI in comparison with 18F-DOPA PET. Eur J Nucl Med Mol Imaging. 2017;44:2084–93.
8. Morana G, Piccardo A, Puntoni M, Nozza P, Cama A, Raso A, et al. Diagnostic and prognostic value of 18F-DOPA PET and 1H-MR spectroscopy in pediatric supratentorial infiltrative gliomas: a comparative study. Neuro-Oncology. 2015;17:1637–47.
9. Morana G, Piccardo A, Garrè ML, Cabria M, Rossi A. 18F-DOPA uptake of developmental venous anomalies in children with brain tumors. Clin Nucl Med. 2016;41:e351–2.
10. Morana G, Piccardo A, Milanaccio C, Puntoni M, Nozza P, Cama A, et al. Value of 18F-3,4-dihydroxyphenylalanine PET/MR image fusion in pediatric supratentorial infiltrative astrocytomas: a prospective pilot study. J Nucl Med. 2014;55:718–23.
11. Berntsson SG, Falk A, Savitcheva I, Godau A, Zetterling M, Hesselager G, et al. Perfusion and diffusion MRI combined with ^{11}C-methionine PET in the preoperative evaluation of suspected adult low-grade gliomas. J Neuro-Oncol. 2013;11:241–9.
12. Lapin DH, Tsoli M, Ziegler DS. Genomic insights into diffuse intrinsic pontine glioma. Front Oncol. 2017;7:57.
13. Saratsis AM, Kambhampati M, Snyder K, Yadavilli S, Devaney JM, Harmon B, et al. Comparative multidimensional molecular analyses of pediatric diffuse intrinsic pontine glioma reveals distinct molecular subtypes. Acta Neuropathol. 2014;127:881–95.
14. Funato K, Major T, Lewis PW, Allis CD, Tabar V. Use of human embryonic stem cells to model pediatric gliomas with H3.3K27M histone mutation. Science. 2014;346:1529–33.
15. Castel D, Philippe C, Calmon R, Le Dret L, Truffaux N, Boddaert N, et al. Histone H3F3A and HIST1H3B K27M mutations define two subgroups of diffuse intrinsic pontine gliomas with different prognosis and phenotypes. Acta Neuropathol. 2015;130:815–27.
16. Huang TY, Piunti A, Lulla RR, Qi J, Horbinski CM, Tomita T, et al. Detection of histone H3 mutations in cerebrospinal fluid-derived tumor DNA from children with diffuse midline glioma. Acta Neuropathol Commun. 2017;5:28.
17. Panditharatna E, Kilburn LB, Aboian MS, Kambhampati M, Gordish-Dressman H, Magge SN, et al. Clinically relevant and minimally invasive tumor surveillance of pediatric diffuse midline gliomas using patient-derived liquid biopsy. Clin Cancer Res. 2018;24:5850–9.
18. Yeom KW, Mitchell LA, Lober RM, Barnes PD, Vogel H, Fisher PG, et al. Arterial spin-labeled perfusion of pediatric brain tumors. AJNR Am J Neuroradiol. 2014;35:395–401.
19. Dangouloff-Ros V, Deroulers C, Foissac F, Badoual M, Shotar E, Grévent D, et al. Arterial spin labeling to predict brain tumor grading in children: correlations between histopathologic vascular density and perfusion MR imaging. Radiology. 2016;281:553–66.
20. Heiss WD, Raab P, Lanfermann H. Multimodality assessment of brain tumors and tumor recurrence. J Nucl Med. 2011;52:1585–600.
21. Fink JR, Muzi M, Peck M, Krohn KA. Multimodality brain tumor imaging: MR imaging, PET, and PET/MR imaging. J Nucl Med. 2015;56:1554–61.
22. Morana G, Puntoni M, Garrè ML, Massollo M, Lopci E, Naseri M, et al. Ability of (18)F-DOPA PET/CT and fused (18)F-DOPA PET/MRI to assess striatal involvement in paediatric glioma. Eur J Nucl Med Mol Imaging. 2016;43:1664–72.
23. Lequin M, Hendrikse J. Advanced MR imaging in pediatric brain tumors, clinical applications. Neuroimaging Clin N Am. 2017;27:167–90.
24. Keil VC, Hartkamp NS, Connolly DJA, Morana G, Dremmen MHG, Mutsaerts HJMM, et al. Added value of arterial spin labeling

magnetic resonance imaging in pediatric neuroradiology: pitfalls and applications. Pediatr Radiol. 2019;49:245–53.
25. Morana G, Tortora D, Staglianò S, Nozza P, Mascelli S, Severino M, et al. Pediatric astrocytic tumor grading: comparison between arterial spin labeling and dynamic susceptibility contrast MRI perfusion. Neuroradiology. 2018;60:437–46.
26. Novak J, Withey SB, Lateef S, MacPherson L, Pinkey B, Peet AC. A comparison of pseudo-continuous arterial spin labelling and dynamic susceptibility contrast MRI with and without contrast agent leakage correction in paediatric brain tumours. Br J Radiol. 2019;92:20170872.
27. Hipp SJ, Steffen-Smith EA, Patronas N, Herscovitch P, Solomon JM, Bent RS, et al. Molecular imaging of pediatric brain tumors: comparison of tumor metabolism using 18F-FDG-PET and MRSI. J Neuro-Oncol. 2012;109:521–7.
28. Hourani R, Horska´ A, Albayram S, Brant LJ, Melhem E, Cohen KJ, et al. Proton magnetic resonance spectroscopic imaging to differentiate between nonneoplastic lesions and brain tumors in children. J Magn Reson Imaging. 2006;23:99–107.
29. Law I, Albert NL, Arbizu J, Boellaard R, Drzezga A, Galldiks N, et al. Joint EANM/EANO/RANO practice guidelines/SNMMI procedure standards for imaging of gliomas using PET with radiolabelled amino acids and [18F]FDG: version 1.0. Eur J Nucl Med Mol Imaging. 2019;46:540–57.
30. Barker PB, Bizzi A, De Stefano N, Gullapalli R, Lin DM. MR spectroscopy in brain tumors. In: Barker PB, Bizzi A, De Stefano N, Gullapalli R, Lin DM, editors. Clinical MR spectroscopy: techniques and applications. New York: Cambridge University Press; 2010. pp 61–90.
31. Alsop DC, Detre JA, Golay X, Günther M, Hendrikse J, Hernandez-Garcia L, et al. Recommended implementation of arterial spin-labeled perfusion MRI for clinical applications: a consensus of the ISMRM perfusion study group and the European consortium for ASL in dementia. Magn Reson Med. 2015;73:102–16.